Inorganic Chemistry

Article

pubs.acs.org/IC

Electronic Structure and Bonding in Iron(II) and Iron(I) Complexes Bearing Bisphosphine Ligands of Relevance to Iron-Catalyzed C−C Cross-Coupling

Jared L. Kneebone, Valerie E. Fleischauer, Stephanie L. Daifuku, Ari A. Shaps, Joseph M. Bailey, Theresa E. Iannuzzi, and Michael L. Neidig*

Department of Chemistry, University of Rochester, Rochester, New York 14627, United States

Supporting Information

ABSTRACT: Chelating phosphines are effective additives and supporting ligands for a wide array of iron-catalyzed cross-coupling reactions. While recent studies have begun to unravel the nature of the in situ-formed iron species in several of these reactions, including the identification of the active iron species, insight into the origin of the differential effectiveness of bisphosphine ligands in catalysis as a function of their backbone and peripheral steric structures remains elusive. Herein, we report a spectroscopic and computational investigation of well-defined $FeCl_2$(bisphosphine) complexes (bisphosphine = SciOPP, dpbz, ^{tBu}dppe, or Xantphos) and known iron(I) variants to systematically discern the relative effects of bisphosphine backbone character and steric substitution on the overall electronic structure and bonding within their iron complexes across oxidation states implicated to be relevant in catalysis. Magnetic circular dichroism (MCD) and density functional theory (DFT) studies demonstrate that common *o*-phenylene and saturated ethyl backbone motifs result in small but non-negligible perturbations to $10Dq(T_d)$ and iron−bisphosphine bonding character at the iron(II) level within isostructural tetrahedra as well as in five-coordinate iron(I) complexes $FeCl(dpbz)_2$ and $FeCl(dppe)_2$. Notably, coordination of Xantphos to $FeCl_2$ results in a ligand field significantly reduced relative to those of its iron(II) partners, where a large bite angle and consequent reduced iron−phosphorus Mayer bond orders (MBOs) could play a role in fostering the unique ability of Xantphos to be an effective additive in Kumada and Suzuki−Miyaura alkyl−alkyl cross-couplings. Furthermore, it has been found that the peripheral steric bulk of the SciOPP ligand does little to perturb the electronic structure of $FeCl_2$(SciOPP) relative to that of the analogous $FeCl_2$(dpbz) complex, potentially suggesting that differences in the steric properties of these ligands might be more important in determining in situ iron speciation and reactivity.

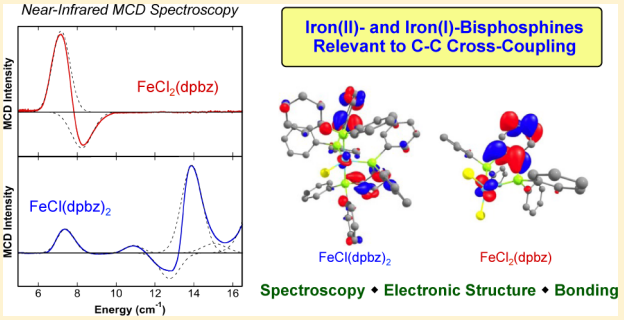

1. INTRODUCTION

The past two decades have witnessed a renaissance in the development of iron-based methods for catalytic C−C bond transformations, motivated by iron's advantageous economic profile and its rich and tunable redox chemistry.[1−6] Following Kochi's seminal reports on iron-catalyzed C−C cross-coupling in the 1970s using simple iron salts,[7−11] recent research efforts have focused on the effects of additives on reaction efficiency and product distributions, demonstrating the efficacy of molecules such as TMEDA,[12−15] N-heterocyclic carbenes (NHCs),[16−21] and bisphosphines[16,22−25] as effective additives in various coupling reactions (e.g., Suzuki−Miyaura, Kumada, and Negishi). Recent work has also demonstrated the utility of well-defined, isolable ferrous complexes bearing bisphosphine supporting ligands of varying steric bulk (e.g., SciOPP,[26−29] dpbz,[22,30,31] and dppe[32,33]) as effective precatalysts in the cross-coupling of aryl nucleophiles with various alkyl and benzyl electrophilic substrates (Scheme 1). Furthermore, both Nakamura and Chai reported the successful coupling of sp^3 carbon centers using ferric and ferrous salts in conjunction with the chelating phosphine Xantphos in the cross-coupling of alkyl borates[25] and Grignards[24] with primary alkyl halides. Recent studies have also continued to expand the breadth of available iron-catalyzed cross-couplings, including the work of Jacobi von Wangelin and co-workers on iron-catalyzed cross-couplings of alkynyl acetates,[34] allylations of aryl Grignards,[35] and reductive aryl−alkenyl cross-coupling reactions.[36]

Despite the advances in developing efficient and selective bisphosphine-supported iron cross-coupling methods, insight into how specific bisphosphines affect iron electronic structure and reactivity remains largely undefined. Such considerations are important because the bisphosphine ligand that is effective for a particular cross-coupling reaction may be ineffective in other reactions (Scheme 1). For example, in the Suzuki−Miyaura coupling of phenyl borates with secondary alkyl

Received: October 6, 2015

DOI: 10.1021/acs.inorgchem.5b02263
Inorg. Chem. XXXX, XXX, XXX−XXX

Scheme 1. Examples of Iron-Bisphosphine-Catalyzed Cross-Coupling Reactions

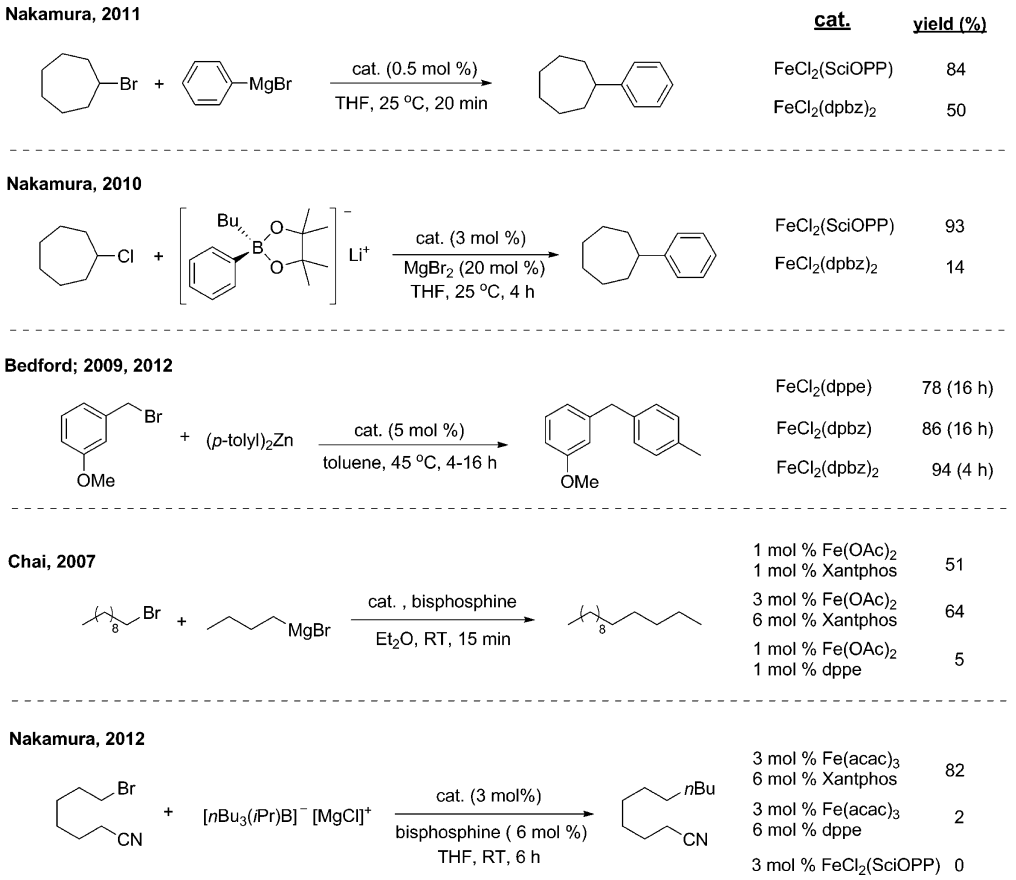

halides developed by Nakamura and co-workers, product yields of >90% and excellent selectivity can be achieved under ambient conditions using $FeCl_2$(SciOPP) as a precatalyst whereas use of the less sterically demanding dpbz ligand within the well-defined $FeCl_2(dpbz)_2$ precatalyst results in a significantly diminished yield and a high recovery of starting material.[26] By contrast, simpler bisphosphines such as dpbz and dppe have been shown by Bedford and co-workers to aid aryl−benzyl Negishi couplings favorably upon stabilization of ferrous precatalysts.[24−26] It should be noted that no examples of effective iron-catalyzed alkyl−alkyl couplings using one of the more widely applied SciOPP, dpbz, or dppe ligands and/or additives exist, suggesting Xantphos may allow the generation of distinct reactive catalytic intermediates relative to the other bisphosphine ligands.[24,25]

These important reactivity differences combined with our recent work on elucidating the identity, electronic structure, and reactivity of transmetalated intermediates within iron-SciOPP-catalyzed aryl−alkyl coupling systems[37,38] motivated the extension of our spectroscopic and theoretical studies to the evaluation of the effect of catalytically relevant bisphosphine supporting ligands on electronic structure and bonding present in nontransmetalated iron(II) and iron(I) species. The catalytically relevant bisphosphines highlighted in Scheme 1 differ structurally in their backbone linkages and rigidity as well as peripheral steric substitution. To date, there has been no systematic investigation of the relative effects of these structural characteristics on resulting coordination compounds with iron in these oxidation states, and by extension, there has yet to be discussion of how these similarities or differences may ultimately contribute to reactivity. In the study presented here, we have sought to address this understudied area by elucidating electronic structure and bonding in a series of well-defined, monomeric, nontransmetalated four-coordinate iron(II) species bearing bisphosphine ligands with catalytically relevant structural motifs utilizing magnetic circular dichroism (MCD) and ^{57}Fe Mössbauer spectroscopies combined with density functional theory (DFT). We further extend this experimental and theoretical analysis to documented five-coordinate Fe(I) species complexes of dpbz and dppe, namely, $FeCl(dpbz)_2$ and $FeCl(dppe)_2$, respectively, to evaluate the effect of bisphosphine ligands in lower-valent iron species with structures of relevance to application as precatalysts in C−C coupling reactions. The results obtained from these studies provide the first quantitation of the effects of bisphosphine backbone structure and peripheral steric substitution on ligand field (LF) strengths and orbital compositions as a function of oxidation state and coordination number, which provide initial insight into the possible effects of these properties on reported differences in cross-coupling activity as a function of bisphosphine ligand.

2. RESULTS AND ANALYSIS

2.1. Structural Characterization of $FeCl_2$(Bisphosphine) Complexes. The effectiveness of the chelating phosphines SciOPP, dpbz, dppe, and Xantphos in promoting C−C cross-coupling catalysis combined with their varied backbone and substitutional character heightened our interest in comparing the electronic structure of their iron compounds within a specific oxidation state. To date, the only

DOI: 10.1021/acs.inorgchem.5b02263
Inorg. Chem. XXXX, XXX, XXX−XXX

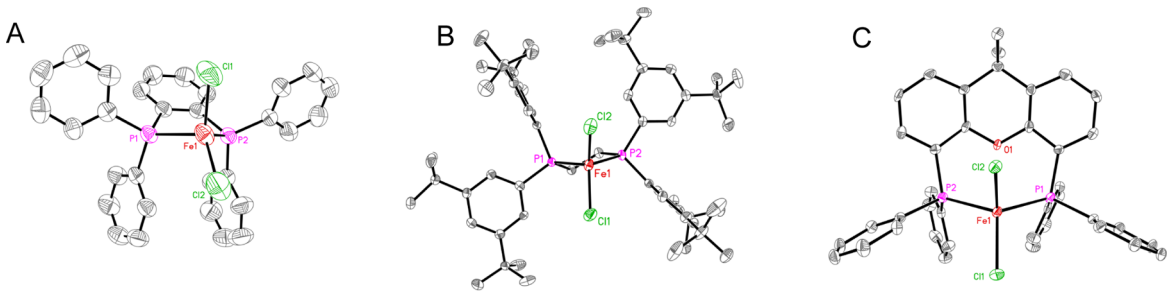

Fe1-P1 (Å)	2.4389(7)	Fe1-P1 (Å)	2.4291(9)	Fe1-P1 (Å)	2.4564(13)
Fe1-P2 (Å)	2.4330(7)	Fe1-P2 (Å)	2.4549(9)	Fe1-P2 (Å)	2.4572(13)
Fe1-Cl1 (Å)	2.2190(8)	Fe1-Cl1 (Å)	2.2120(10)	Fe1-Cl1 (Å)	2.2137(12)
Fe1-Cl2 (Å)	2.2132(8)	Fe1-Cl2 (Å)	2.2225(10)	Fe1-Cl2 (Å)	2.2548(12)
P1-Fe1-P2 (°)	80.38(3)	P1-Fe1-P2 (°)	82.85(3)	P1-Fe1-P2 (°)	109.30(4)
Cl1-Fe1-Cl2(°)	124.85(4)	Cl1-Fe1-Cl2(°)	120.65(4)	Cl1-Fe1-Cl2(°)	122.12(5)

Figure 1. X-ray crystal structures with selected bond length and angle metrics of (A) $FeCl_2$(dpbz), (B) $FeCl_2$(^{tBu}dppe), and (C) $FeCl_2$(Xantphos). Structures are shown with thermal ellipsoids at the 50% probability level, and hydrogen atoms have been omitted for the sake of clarity. For $FeCl_2$(Xantphos), one of the two independent molecules in the asymmetric unit is pictured and highlighted metrically.

Table 1. Summary of Ligand Field, Spin Hamiltonian, and Solid State 80 K ^{57}Fe Mössbauer Parameters for $FeCl_2$(Bisphosphine) Complexes

	NIR and VTVH MCD						Mössbauer	
complex	LF bands (cm^{-1})	$10Dq(T_d)$ (cm^{-1})	D (cm^{-1})	$\lvert E/D\rvert$[a]	δ (cm^{-1})	$g_{\lVert}$	δ (mm/s)	ΔE_Q (mm/s)
$FeCl_2$(SciOPP)	7160, 8140	7650	−8 ± 2	0.31	2.1 ± 0.2	8.2 ± 0.2	0.73	2.54
$FeCl_2$(dpbz)	7170, 8230	7700	−9 ± 2	0.29	2.3 ± 0.2	8.3 ± 0.2	0.73	2.49
$FeCl_2$(^{tBu}dppe)	6710, 7670	7190	−7 ± 2	0.33	2.3 ± 0.2	8.3 ± 0.2	0.73	2.82
$FeCl_2$(Xantphos)	5160, 7100	6130	−10 ± 2	0.22	1.4 ± 0.2	8.2 ± 0.2	0.75	2.67

[a]The error bars for the $\lvert E/D\rvert$ values are ± 0.02, with a maximum possible value of $\lvert E/D\rvert$ of 0.33.

structurally characterized monomeric 1:1 ferrous adduct incorporating these ligands is $FeCl_2$(SciOPP), developed by Nakamura and co-workers. Because structurally characterized complexes of the type $FeCl_2$(PP) (PP = bidentate phosphine ligation) have been widely reported,[39−44] we envisioned an isostructural series of four-coordinate ferrous dihalides as a set of model compounds to begin to systematically discern how different structural characteristics of the chelating phosphine affect the overall electronic structure and bonding within their coordination compounds at the iron(II) level. While the preparation of $FeCl_2$(dpbz) has been summarized in the literature using stoichiometric equivalents of dpbz and $FeCl_2$,[30] no solid state characterization of this adduct has been reported. Reaction of dpbz and $FeCl_2(THF)_{1.5}$ in hot toluene followed by slow cooling to −30 °C resulted in the isolation of crystals suitable for X-ray diffraction analysis. Extension of these synthetic efforts to the Xantphos ligand resulted in isolation of the desired $FeCl_2$(Xantphos) complex, with single crystals obtained from the slow evaporation of a concentrated THF solution of the complex. The solid state structures of $FeCl_2$(dpbz) and $FeCl_2$(Xantphos) are depicted in Figure 1.

Both $FeCl_2$(dpbz) and $FeCl_2$(Xantphos) are characterized by a distorted tetrahedral iron center, consistent with the observed difference between the P−Fe−P and Cl−Fe−Cl angles within each complex. The differences between these angle metrics within a specific complex are most pronounced for $FeCl_2$(dpbz) and $FeCl_2$(SciOPP), in which the rigid *o*-phenylene linkage of both dpbz and SciOPP constrain the P−Fe−P angle to 80.38° and 80.63°, respectively. While the larger Cl−Fe−Cl angles in these two species [124.85° for $FeCl_2$(dpbz) and 122.16° for $FeCl_2$(SciOPP)] compare well with that of $FeCl_2$(Xantphos) (122.12°), the additional width of the xanthene linker in the latter species results in a much larger P−Fe−P angle (bite angle) of 109.30°. This bite angle magnitude compares well with those of the known first row metal adducts $CoCl_2$(Xantphos)[45] and $NiCl_2$(Xantphos).[46]

Isolation of a monomeric four-coordinate ferrous adduct bearing catalytically relevant dppe was, in contrast, unattainable because of the increased flexibility of the backbone. Langer and co-workers recently demonstrated the prevalence of a bridging dppe coordination motif when combined with equimolar amounts of $FeCl_2$,[47] isolating the coordination polymer [μ-(dppe)$FeCl_2$]$_n$. Having isolated the same polymeric material when attempting the equimolar combination of dppe with $FeCl_2$ under separate reaction conditions,[48] we explored a more sterically encumbered ligand structure to overcome the preference of such a flexible bisphosphine to support polymeric structures. Incorporating the bulky 3,5-di-*tert*-butyl substitution of Nakamura's SciOPP ligand into a bisphosphine scaffold bearing a saturated ethyl backbone, we synthesized 1,2-bis(3,5-di-*tert*-butylphenylphosphino)ethane (^{tBu}dppe) and investigated its coordination to $FeCl_2$. The monomeric complex $FeCl_2$(^{tBu}dppe) was synthesized through the reaction of equimolar amounts of (^{tBu}dppe) with $FeCl_2(THF)_{1.5}$ in refluxing 2-propanol, and X-ray quality single crystals were isolated from slow evaporation of a concentrated 1,4-dioxane solution at room temperature. The bond length metrics of the crystal structure are very similar to those of the analogous complexes bearing SciOPP, dpbz, and Xantphos ligands with Fe−P distances of 2.429 and 2.455 Å and Fe−Cl distances of

DOI: 10.1021/acs.inorgchem.5b02263
Inorg. Chem. XXXX, XXX, XXX−XXX

2.212 and 2.223 Å (Figure 1). The P−Fe−P angle of 82.85° is larger than those observed for $FeCl_2$(SciOPP) and $FeCl_2$(dpbz), and the Cl−Fe−Cl angle of 120.65° is slightly reduced by comparison.

2.2. Spectroscopic Characterization of $FeCl_2$(Bisphosphine) Complexes. With access to a series of distorted tetrahedral bisphosphine-supported ferrous dihalide complexes, ^{57}Fe Mössbauer and MCD spectroscopic investigations were performed to probe the effects of bisphosphine backbone character and peripheral steric substitution on the overall electronic structure of their adducts with $FeCl_2$. For $FeCl_2$(SciOPP), solid state ^{57}Fe Mössbauer analysis yields a single quadrupole doublet with parameters of δ = 0.73 mm/s and ΔE_Q = 2.54 mm/s, consistent with a high-spin Fe(II) distorted tetrahedron (Table 1 and Figure S1). The 5 K, 7 T near-infrared (NIR) MCD spectrum of $FeCl_2$(SciOPP) is described by two LF transitions at low energy, a positive band at 7160 cm^{-1} and a negative band at 8140 cm^{-1} (Figure 2A). While LF theory predicts a single spin-allowed transition in T_d symmetry (^{5}E → ^{5}T$_2$) for a high-spin S = 2 complex, the presence of two observed LF transitions reflects the distorted nature of the tetrahedron, whereby the difference in transition energy reflects loss of degeneracy from the ^{5}T$_2$ excited state. From these LF transitions, the magnitude of the ligand field is determined to be $10Dq(T_d)$ = 7650 cm^{-1}. Notably, the observed value of $10Dq(T_d)$ in the $FeCl_2$(SciOPP) ligand is larger than those previously reported for the monodentate phosphine complexes $FeCl_2(PPh_3)_2$ [$10Dq(T_d)$ = 6590 cm^{-1}] and $FeCl_2(PMe_3)_2$ [$10Dq(T_d)$ = 6970 cm^{-1}].[49] The LF bands exhibit a pseudo-A term, where the intensity of the transitions derives from two oppositely signed, temperature-dependent C-term absorption features, a spectral profile consistent with the NIR MCD spectra of other Fe(II)-phosphine and bisphosphine distorted tetrahedra studied previously.[37,38,49] Saturation magnetization data collected at 6481 cm^{-1} for $FeCl_2$(SciOPP) (Figure 2A, inset) are described well by an S = 2 non-Kramers doublet model with negative zero-field splitting (ZFS) and ground state spin Hamiltonian parameters of δ = 2.1 ± 0.2 cm^{-1}, $g_{\|}$ = 8.2 ± 0.2 cm^{-1}, axial ZFS parameter D = −8 ± 2 cm^{-1}, and rhombicity $|E/D|$ = 0.31 ± 0.02 (Table 1).

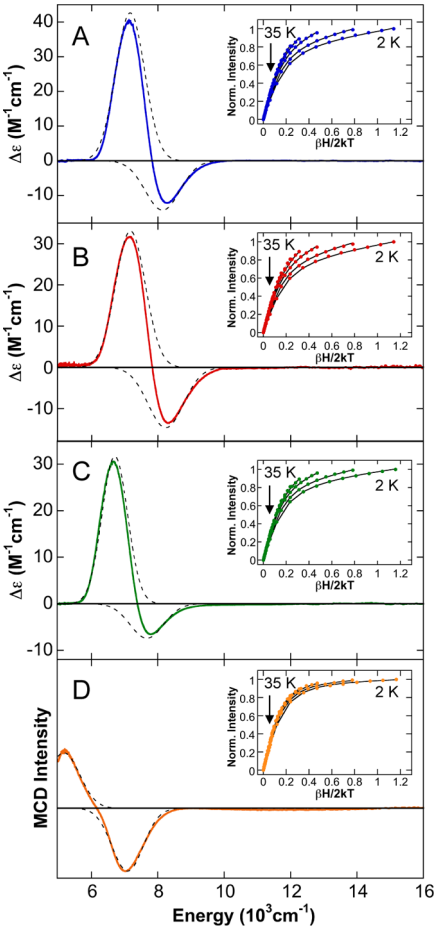

Figure 2. NIR MCD spectra (5 K, 7 T) of (A) $FeCl_2$(SciOPP), (B) $FeCl_2$(dpbz), (C) $FeCl_2$(^{tBu}dppe), and (D) $FeCl_2$(Xantphos). Gaussian fits are given for each spectrum (---). Saturation magnetization data (dots) and best fits (lines) are given in the insets for each species, collected at 6481, 6536, 6061, and 5482 cm^{-1} for $FeCl_2$(SciOPP), $FeCl_2$(dpbz), $FeCl_2$(^{tBu}dppe), and $FeCl_2$(Xantphos), respectively. Saturation magnetization data were collected at 2, 3, 5, 7.5, 10, 15, 25, and 35 K. All spectra were collected in a 6:1 toluene-d_8/benzene-d_6 mixture except for $FeCl_2$(Xantphos), which was collected on a solid mull sample.

The rigid *o*-phenylene linkage between the phosphorus atoms in the SciOPP ligand is shared with dpbz, providing the same conjugated backbone electronic system between the two species, though it is obvious that the two ligands differ greatly in their steric bulk. The similar solid state structural metrics shared by $FeCl_2$(SciOPP) and $FeCl_2$(dpbz) (vide supra) are corroborated by very similar ^{57}Fe Mössbauer parameters, with $FeCl_2$(dpbz) characterized by δ = 0.73 mm/s and ΔE_Q = 2.49 mm/s in the solid state (Table 1). The 5 K, 7 T NIR MCD spectrum of $FeCl_2$(dpbz) exhibits LF transitions at 7170 and 8230 cm^{-1}, yielding a value of $10Dq(T_d)$ = 7700 cm^{-1}, nearly identical to that determined for $FeCl_2$(SciOPP) (Figure 2B). In addition, saturation magnetization data for $FeCl_2$(dpbz) (Figure 2B, inset) are described well by an S = 2 non-Kramers doublet model with ground state spin Hamiltonian parameters (Table 1) very similar to those obtained for $FeCl_2$(SciOPP). The combined spectroscopic investigations highlight the fact that with constant backbone structure, the presence or absence of 3,5-di-*tert*-butyl substitution has little effect on the overall electronic structure of the resulting four-coordinate adducts at the Fe(II) level. More appreciable differences in $10Dq(T_d)$ are observed upon varying the ligand to ^{tBu}dppe and Xantphos. For $FeCl_2$(^{tBu}dppe), observation of LF transitions at 6710 and 7670 cm^{-1} [$10Dq(T_d)$ = 7190 cm^{-1}] by NIR MCD indicates a ligand field smaller than that previously observed for $FeCl_2$(SciOPP) and $FeCl_2$(dpbz). Notably, the magnitude of $10Dq(T_d)$ undergoes an even larger decrease upon ligation of Xantphos to $FeCl_2$, with LF transitions observed at 5160 and 7100 cm^{-1} in the NIR MCD spectrum, corresponding to $10Dq(T_d)$ = 6130 cm^{-1}. Despite this large shift in $10Dq(T_d)$, the Mössbauer isomer shift of $FeCl_2$(Xantphos) (δ = 0.75 mm/s) is observed to remain quite consistent with those of the other complexes in the series. While Mössbauer spectroscopy can be insightful for determining differences in oxidation or spin state among iron species, the results presented here clearly demonstrate that MCD spectroscopy is a higher-resolution method for probing differences in the ligand field of iron species in the same oxidation and spin state. Lastly, the 5 K, 7 T UV−vis MCD spectra of each of the $FeCl_2$(bisphosphine) species contain multiple high-energy charge transfer (CT) transitions (Figure S2) that are assigned and summarized in the Supporting Information using TD-DFT analysis.

DOI: 10.1021/acs.inorgchem.5b02263
Inorg. Chem. XXXX, XXX, XXX−XXX

Table 2. Comparison of Experimental and Calculated Structural Parameters for $FeCl_2$(Bisphosphine) Complexes

	$FeCl_2$(SciOPP)		$FeCl_2$(dpbz)		$FeCl_2$(Xantphos)		$FeCl_2$(^{tBu}dppe)	
	exp	calc	exp	calc	exp	calc	exp	calc
Fe−P1 (Å)	2.463(1)	2.42	2.439(1)	2.41	2.456(2)	2.45	2.429(1)	2.45
Fe−P2 (Å)	2.441(2)	2.41	2.433(1)	2.41	2.457(2)	2.44	2.455(1)	2.44
Fe−Cl1 (Å)	2.219(1)	2.25	2.219(1)	2.24	2.214(1)	2.23	2.212(1)	2.23
Fe−Cl2 (Å)	2.217(2)	2.23	2.213(1)	2.23	2.255(1)	2.23	2.223(2)	2.24
P−Fe−P (deg)	80.63(4)	83.0	80.38(3)	81.9	109.30(4)	108.8	82.85(3)	84.7
Cl−Fe−Cl (deg)	122.16(6)	121.7	124.85(4)	123.6	122.12(5)	128.6	120.65(4)	119.1

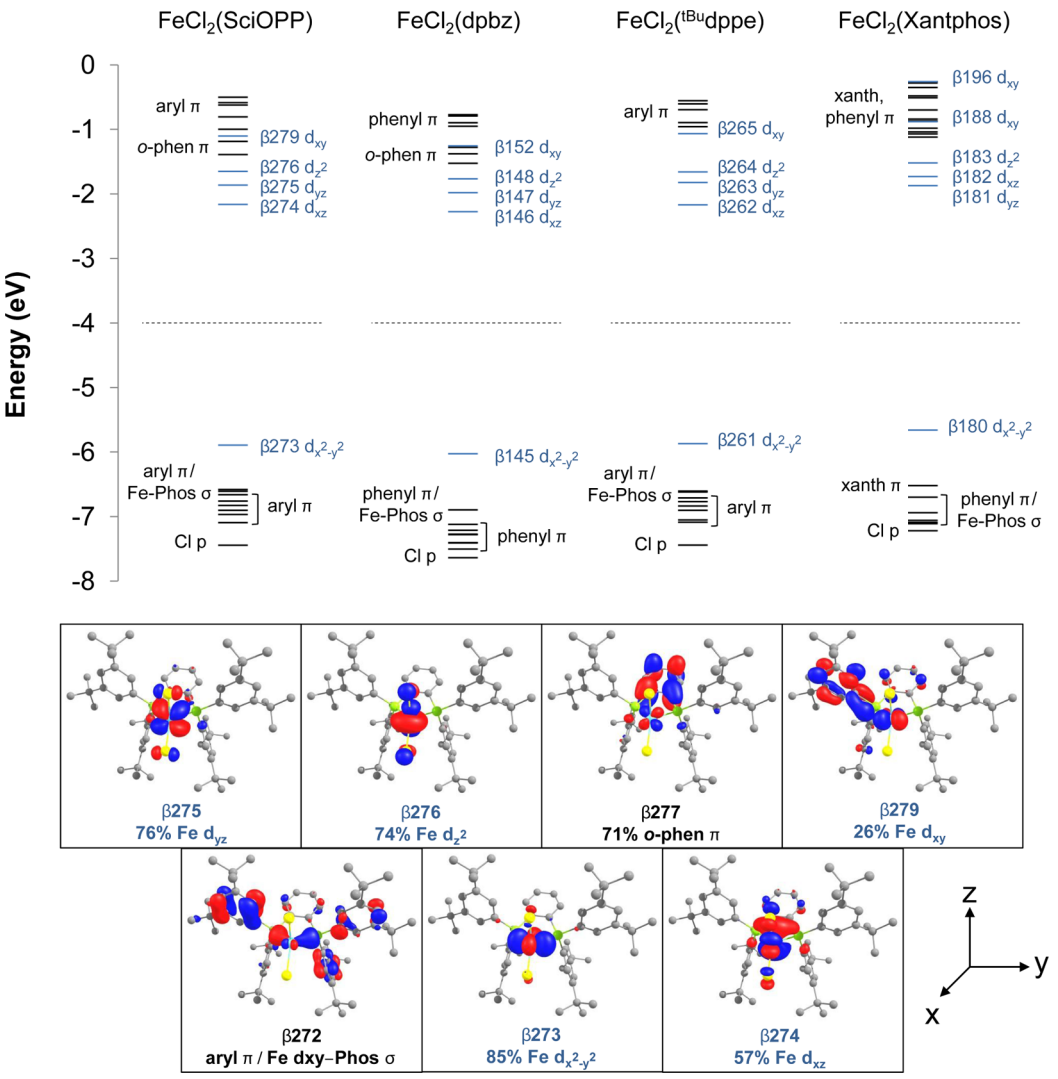

Figure 3. Calculated FMO energy diagrams for $FeCl_2$(bisphosphine) complexes and selected orbital depictions for $FeCl_2$(SciOPP).

2.3. Electronic Structure Calculations of $FeCl_2$(Bisphosphine) Complexes. Spin-unrestricted DFT calculations were used in conjunction with MCD spectroscopy to gain further insight into the effects of bisphosphine backbone and steric substitution on electronic structure and bonding in this series of iron(II) bisphosphine complexes. Geometry optimizations using PBEPBE/TZVP were performed on the crystal coordinates, demonstrating good agreement between experiment and theory (Table 2) with minor contractions of the Fe−P bond distances and slightly elongated Fe−Cl bonds observed in the calculated structures (in solvent models) relative to the crystal structures. Additionally, the order of increasing P−Fe−P angle in the crystal structures is preserved in the optimized geometries: $FeCl_2$(dpbz) < $FeCl_2$(SciOPP) < $FeCl_2$(^{tBu}dppe) < $FeCl_2$(Xantphos).

Evaluations of molecular orbital character and energies were subsequently conducted from the optimized geometries using spin-unrestricted B3LYP/TZVP, placing emphasis on the occupied and unoccupied frontier molecular orbitals (FMOs) of the β manifold to describe the major contributions to bonding. A cumulative β FMO energy level diagram containing all four complexes is shown in Figure 3, accompanied by selected FMO depictions for $FeCl_2$(SciOPP). The FMOs of $FeCl_2$(SciOPP) bear dominant Fe d character in the HOMO (β273, 85% $d_{x^2-y^2}$) as well as in β274 (LUMO), β275 (LUMO +1), β276 (LUMO+2), and β279 (LUMO+5), assigned as d_{xz},

DOI: 10.1021/acs.inorgchem.5b02263
Inorg. Chem. XXXX, XXX, XXX−XXX

d_{yz}, d_{z^2}, and d_{xy}, respectively (also see Figure S5). The highest occupied ligand-based MO lies directly below the $d_{x^2-y^2}$ HOMO in energy (β272), containing Fe d_{xy}/phosphorus p σ bonding interaction character. Orbital contributions in addition to iron d character in the LUMO, LUMO+1, and LUMO+2 derive from mixing with p orbital character of both the chloride ligands and the phosphorus atoms of the SciOPP ligand. Increased orbital covalency is found in the LUMO (57% Fe d_{xz}) due to an increased level of mixing with phosphorus p character and an elevated Fe−P overlap population relative to the other Fe d-based MOs. An increased level of mixing in the d_{xy}-based β279 (LUMO+5, 26% d_{xy}) originates from elevated intra-aryl π character, present as the major component of the orbital description. Notably, a consecutive energy ordering of unoccupied d-based FMOs is disrupted by low-lying ligand-based orbitals β277 and β278. In these orbitals, high degrees of intraligand π bonding and antibonding interactions in the conjugated *o*-phenylene backbone are observed, and thus, ligand-based character dominates the orbital descriptions. The stabilization of these ligand-based acceptor MOs is consistent with the FMO description of the analogous *o*-phenylene-linked $FeCl_2$(dpbz) (vide infra) and has also been observed in the MO compositions of mono- and bis-mesitylated Fe(II)-SciOPP species.[37]

FMO analysis of the remainder of the series of iron(II) bisphosphine complexes results in a very similar description of Fe d-based MOs, with $FeCl_2$(dpbz), $FeCl_2$(^{tBu}dppe), and $FeCl_2$(Xantphos) each possessing a HOMO of dominant Fe $d_{x^2-y^2}$ character and high-lying d_{xy}-based MOs (Figure 3 and Figures S6−S8). Notably, the d_{xy}-derived MOs are mixed to a lesser degree for $FeCl_2$(dpbz) (β152) and $FeCl_2$(^{tBu}dppe) (β265) than in $FeCl_2$(Xantphos), the latter bearing two unoccupied FMOs of very similar d_{xy} character (β188, 22%; β196, 25%). While $FeCl_2$(SciOPP), $FeCl_2$(dpbz), and $FeCl_2$(^{tBu}dppe) contain the same cumulative d orbital energy ordering, $FeCl_2$(Xantphos) possesses a more destabilized d_{xz} orbital, pushing it to an energy higher than that of d_{yz}. Analogous to $FeCl_2$(SciOPP), each additional complex in the series bears high-lying occupied ligand-based MOs characterized by Fe−P σ bonding interactions, where these MOs are slightly more stabilized in $FeCl_2$(dpbz) and $FeCl_2$(Xantphos). The most notable deviations in FMO descriptions across the iron(II) complexes occur in the nature of their low-lying ligand-based acceptor orbitals, an effect that is a direct consequence of the nature of the ligand backbone structure. As seen in Figure 3 and Figures S6−S8, MOs bearing high degrees of π character within the conjugated *o*-phenylene backbone of $FeCl_2$(SciOPP) (β277, β278, and β280) and $FeCl_2$(dpbz) (β149, β150, and β151) are more energetically stabilized than the unoccupied ligand-based FMOs of $FeCl_2$(^{tBu}dppe) in which π MO character resides only in the conjugated systems of the aryl substituents. Intermediate stabilization of unoccupied ligand-based MOs is observed in $FeCl_2$(Xantphos), in which increased π density in the extended xanthene system combined with phenyl π character imparts sufficient stability to push these MOs closer in energy to Fe d_{z^2} (β183) than is observed in $FeCl_2$(^{tBu}dppe) (Figure S8).

Mayer bond order (MBO) analyses were also conducted across the series of Fe(II) bisphosphine complexes, the results of which are shown in Table 3. The calculated magnitudes of Fe−P MBOs trend with the experimental magnitude of $10Dq(T_d)$ obtained from NIR MCD (vide supra), where reduced Fe−P bond orders indicate a weaker Fe−P interaction, reduced Fe−P bond covalency, and, hence, lower values of $10Dq(T_d)$. Additionally, increased Fe−P bond orders are found to be accompanied by a general decrease in the overall Fe−Cl bond orders of the complexes. Overall, the FMO descriptions and MBO analysis support the spectroscopic observations that $FeCl_2$(SciOPP) and $FeCl_2$(dpbz) are very similar with respect to their electronic structure and bonding, despite the peripheral steric bulk present in the SciOPP ligand structure. In contrast, $FeCl_2$(Xantphos) is observed to have the most distinct electronic structure and bonding characteristics of the complexes present in this iron(II) bisphosphine series.

Table 3. Calculated Mayer Bond Orders for $FeCl_2$(Bisphosphine) Complexes

	Mayer bond orders	
complex	Fe−P	Fe−Cl
$FeCl_2$(SciOPP)	0.707, 0.711	0.823, 0.854
$FeCl_2$(dpbz)	0.706, 0.707	0.831, 0.852
$FeCl_2$(^{tBu}dppe)	0.693, 0.680	0.864, 0.833
$FeCl_2$(Xantphos)	0.670, 0.669	0.867, 0.854

2.4. Electronic Structure and Bonding in Iron(I) Bisphosphine Complexes. Recent reports by Bedford and co-workers have highlighted the use of well-defined low-spin five-coordinate iron(I) bisphosphine complexes supported by dpbz and dppe ligands as precatalysts in the Negishi coupling of benzyl substrates with aryl nucleophiles.[31,32] The implication of iron(I) as a potentially catalytically relevant oxidation state within these C−C cross-coupling reactions motivated the extension of the approach described above to understanding the effects of a supporting bisphosphine ligand on the electronic structure and bonding at iron in the +1 oxidation state. While well-defined iron(I) bisphosphines with ligands relevant to cross-coupling are rare, $FeCl(dppe)_2$ and $FeCl(dpbz)_2$ provide a firm starting point for evaluating the effects of bisphosphine backbone structure on electronic structure and bonding at the iron(I) oxidation state. NIR MCD analyses of both species yield rich LF spectra in which six d−d transitions can be resolved (Figure 4), consistent with their low-spin nature and the resulting spin-allowedness of both α and β transitions for these $S = {}^1/_2$ species. TD-DFT analysis of the LF spectra predicts high degrees of mixing within the transitions,

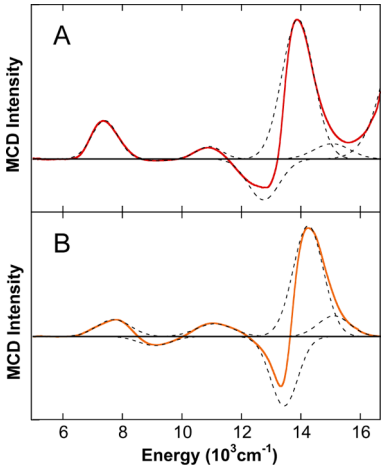

Figure 4. NIR MCD spectra (5 K, 7 T) of (A) $FeCl(dpbz)_2$ and (B) $FeCl(dppe)_2$. Spectra were collected in a 6:1 toluene-d_8/benzene-d_6 mixture.

DOI: 10.1021/acs.inorgchem.5b02263
Inorg. Chem. XXXX, XXX, XXX−XXX

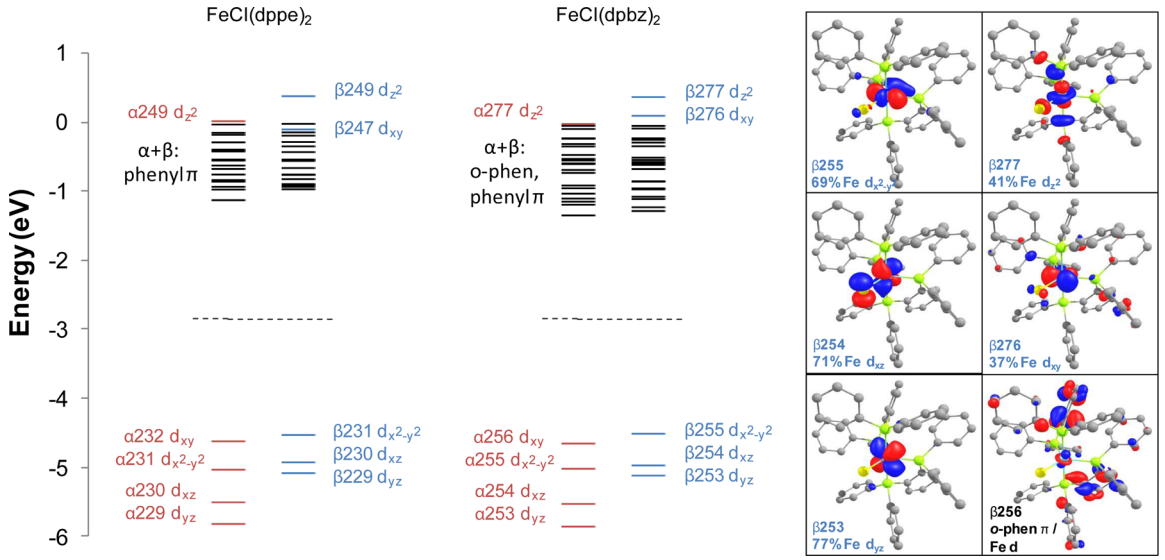

Figure 5. Calculated FMO energy diagrams for $FeCl(dppe)_2$ and $FeCl(dpbz)_2$ and selected orbital depictions for $FeCl(dpbz)_2$.

and the experimentally observed shift of the LF transitions to slightly higher energies in the case of $FeCl(dppe)_2$ relative to $FeCl(dpbz)_2$ demonstrates a slightly increased ligand field in the case of the former. UV−vis MCD analysis of both complexes results in similar CT profiles, with TD-DFT used to assign Fe d → phenyl/*o*-phen π MLCT as the dominant transition character between 16000 and 32000 cm^{-1} (Figure S3). The experimental CT regions are consistent with the presence of a large number of low-lying ligand-based π acceptor FMOs (Figure 5).

The highest-lying occupied MOs in both the α and β manifolds for $FeCl(dppe)_2$ and $FeCl(dpbz)_2$ are characterized by increased Fe d character (Figure 5). The β manifold of each complex is described by HOMOs of $d_{x^2-y^2}$ character [β231 for $FeCl(dppe)_2$ and β255 for $FeCl(dpbz)_2$] with lower-lying d_{yz} and d_{xz} orbitals at β229 and β230, respectively, for $FeCl(dppe)_2$ and β253 and β254, respectively, in the case of $FeCl(dpbz)_2$. A consecutive ordering of α and β Fe d-based MOs is broken in the case of both complexes by low-lying ligand-derived π acceptor orbitals. In the case of $FeCl(dpbz)_2$, π orbital density located on the *o*-phenylene backbone of the dpbz ligands results in α and β LUMO energies lower than those of $FeCl(dppe)_2$. This is consistent with observed energy differences between ligand-based acceptor orbitals at the iron(II) level upon variation of ligand backbone saturation (vide supra). MBO calculations result in an increased average Fe−P MBO in $FeCl(dppe)_2$ (0.981) relative to that of $FeCl(dpbz)_2$ (0.968), consistent with the generally shorter Fe−P bond distances in both the crystal and DFT-optimized structure in $FeCl(dppe)_2$ and its slightly larger LF magnitude obtained from NIR MCD. Overall, the electronic structure calculations on these bisphosphine-supported complexes corroborate the experimental observations that the differences in backbone saturation in dppe and dpbz result in an observable but small effect on the overall electronic structure and bonding at the iron(I) level, in turn indicating that the nature of the bisphosphine ligand in analogous five-coordinate halides likely has little effect on the reactivity of the starting precatalyst.

3. DISCUSSION

The application of bisphosphines as additives and supporting ligands in iron-catalyzed C−C cross-coupling catalysis has resulted in numerous reports of efficient and selective reaction methodologies. An attractive feature of these molecules is the ability to tune their backbone electronic properties and peripheral steric structure to access new ligand architectures. Despite the reported differences in reactivity of catalytic systems as a function of bisphosphine ligand, no systematic investigation of the effects of bisphosphine ligand structural variations on electronic structure and bonding of well-defined iron complexes has been reported. In this study, we have utilized a combination of MCD spectroscopic investigations and DFT studies to obtain insight into electronic structure and bonding in iron(II) and iron(I) species containing bisphosphine ligand structures relevant to iron-catalyzed cross-coupling, thus focusing on analysis of iron oxidation states proposed to be relevant as on-cycle active species in catalysis.

From this study, the following effects of bisphosphine structural variations on resulting iron-bisphosphine electronic structure and bonding have been determined. (1) The presence of *o*-phenylene (SciOPP and dpbz) versus ethyl (^{tBu}dppe and dppe) backbones in bisphosphine ligands has a minor but non-negligible effect on electronic structure and bonding in both iron(II) and iron(I) bisphosphine complexes. At the iron(II) level, the presence of an ethyl linker in $FeCl_2(^{tBu}dppe)$ results in a small decrease in $10Dq(T_d)$ relative to those of the corresponding SciOPP and dpbz complexes. The most notable effects of backbone saturation exist in the characterization of excited states, where the lack of a conjugated ligand backbone in $FeCl_2(^{tBu}dppe)$ results in higher-lying ligand-based acceptor MOs as characterized by MO calculations and experimental CT analysis. Similarly, at the iron(I) level, varying the saturation of the bisphosphine backbone in $FeCl(dppe)_2$ and $FeCl(dpbz)_2$ results in minor differences in electronic structure and bonding. Chelation of dppe leads to a small increase in LF, ligand-based acceptor MOs of slightly higher energy and slightly higher-energy MLCT transitions for $FeCl(dppe)_2$ than for $FeCl(dpbz)_2$. (2) The introduction of peripheral steric bulk in bisphosphines with *o*-phenylene backbones (SciOPP and dpbz) has minimal effects on iron(II)-bisphosphine electronic

DOI: 10.1021/acs.inorgchem.5b02263
Inorg. Chem. XXXX, XXX, XXX−XXX

structure and bonding. Nearly identical LF splittings and MO compositions and energies are observed for $FeCl_2$(SciOPP) and $FeCl_2$(dpbz), indicating that the introduction of the 3,5-di-*tert*-butyl substitution pattern in SciOPP does not result in structural distortions that significantly perturb the overall electronic structure and bonding at iron relative to the less bulky dpbz ligand. (3) Xantphos ligation at the iron(II) level results in a distinctly different iron−phosphorus bonding and electronic structure description compared to those of the other ferrous bisphosphine complexes employed in this study. The magnitude of $10Dq(T_d)$ in $FeCl_2$(Xantphos) is significantly reduced compared to the magnitudes of those of $FeCl_2$(SciOPP) and $FeCl_2$(dpbz), correlating with the lowest overall iron−phosphorus MBOs in the series.

Studies of the effects of bisphosphine ligands on electronic structure and bonding in transmetalated, active iron-bisphosphine species are required to definitively correlate such effects to differences in reactivity. However, the observed similarities and differences in electronic structure and bonding within nontransmetalated iron complexes coordinating catalytically relevant bisphosphine scaffolds do provide some preliminary insight into potential contributions of bisphosphine ligands to reactivity. For example, Xantphos is the only bisphosphine ligand shown to date to be effective in promoting iron-catalyzed Kumada and Suzuki−Miyaura alkyl−alkyl cross-couplings.[18,19] The difference in effects of the molecular structure of Xantphos on electronic structure and iron−phosphorus bonding in ferrous Xantphos adducts relative to isostructural adducts supported by *o*-phenylene and ethyl backbone linkers is likely a significant contributor to the unique cross-coupling reactivities observed, potentially functioning to govern the extent of reduction accessible in Xantphos-supported intermediates and helping to mitigate β hydrogen elimination within in situ-formed species. Furthermore, both dpbz and dppe have been shown by Bedford and co-workers to be effective for iron-catalyzed Negishi cross-couplings of aryl nucleophiles and benzyl halides despite their significant differences in backbone structure.[24−26] While the question of whether iron(I) or iron(II) active species are functional in these catalytic systems is still to be answered, the studies herein demonstrate that small differences in electronic structure and bonding result from chelation of *o*-phenylene and ethyl-bridged bisphosphines at both oxidation state levels. Combined with the observation of comparable catalytic activity by Bedford and co-workers for iron(I) precatalysts bearing dpbz and dppe, this observation appears to suggest that the small electronic structure and bonding differences resulting from *o*-phenylene versus ethyl backbones may not have a significant effect in these reactions. Lastly, it is interesting to note that disparities in reactivity reported in the literature using well-defined SciOPP- and dpbz-supported precatalysts in Kumada and Suzuki−Miyaura cross-couplings of phenyl nucleophiles and secondary alkyl halides do exist despite their nearly identical electronic and orbital descriptions in four-coordinate ferrous dichloride complexes as determined herein.[26,27] Thus, it may be that the steric variations present in these ligands are more important for dictating catalytic performance by altering in situ iron speciation. In fact, evidence of such sterically driven effects on iron speciation has already been reported on the basis of the nature of the reduced iron species observed to form in situ with SciOPP and dpbz ligands. In reactions of $FeCl_2$(SciOPP) with phenyl nucleophiles, it has been shown that the dominant reduced iron species is Fe(η^6-biphenyl) (SciOPP), formed via reductive elimination of a mononuclear, bisphenylated iron(II)-SciOPP species.[38] By contrast, 2:1 ferrous adducts can be easily accessed with the less sterically bulky dpbz and used as precursors to generate bis-chelated $FeX(dpbz)_2$ (X = Cl, Br, or *p*-tolyl) iron(I) species through stoichiometric treatment with Grignard or organozinc nucleophiles.[31] In fact, efforts in our lab to isolate the analogous iron(I) SciOPP species, $FeBr(SciOPP)_2$, have resulted in only the monochelated bridged iron(I) dimer $[FeBr(SciOPP)]_2$ being accessible upon reduction of $FeBr_2$(SciOPP) with KC_8 (Figure 6), consistent with the fact that no 2:1 adduct of SciOPP to iron has yet been reported for iron in any oxidation state.

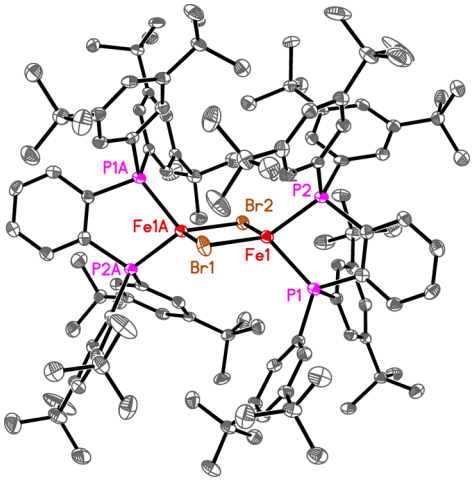

Figure 6. X-ray crystal structure of $[FeBr(SciOPP)]_2$ shown with thermal ellipsoids at the 50% probability level. Hydrogen atoms and cocrystallized solvent (Et_2O) have been omitted for the sake of clarity.

4. CONCLUSIONS

In this study, the combination of MCD and DFT studies has provided direct insight into the effects of bisphosphine ligand structural variations in ligands utilized in iron-catalyzed cross-coupling on iron-bisphosphine electronic structure and bonding in both iron(II) and iron(I) complexes. Interestingly, the unique cross-coupling reactivity observed employing Xantphos is found to correlate with distinct differences in electronic structure and bonding with this ligand compared to other bisphosphines employed in iron-catalyzed cross-coupling bearing *o*-phenylene or saturated ethyl backbone linkages. The analogous reactivities in Negishi cross-couplings with dppe and dpbz combined with the small but non-negligible differences in electronic structure and bonding observed herein in both their iron(II) and iron(I) complexes appear to suggest that electronic structure and bonding effects of *o*-phenylene versus ethyl backbones may not have a significant effect in these reactions. Furthermore, it has been found that the peripheral steric bulk of the SciOPP ligand does little to perturb the electronic structure of $FeCl_2$(SciOPP) relative to the analogous $FeCl_2$(dpbz) complex, potentially suggesting that differences in the steric properties of these ligands might be more important in determining catalytic performance in these systems. Extension of these electronic structure studies to additional iron-bisphosphine species, including series of transmetalated species as a function of bisphosphine ligand, should continue to expand our understanding of ligand structural variations on reactivity in cross-couplings utilizing iron-bisphosphines.

DOI: 10.1021/acs.inorgchem.5b02263
Inorg. Chem. XXXX, XXX, XXX−XXX

5. EXPERIMENTAL SECTION

5.1. General Considerations. All reagents were purchased from commercial sources. All air and moisture sensitive synthetic manipulations were performed using an MBraun inert atmosphere (N_2) drybox or by standard Schlenk techniques. All preparations of spectroscopy samples were conducted in an MBraun inert atmosphere (N_2) drybox equipped with a direct liquid nitrogen inlet line. Anhydrous solvents were further dried using activated alumina, 4 Å molecular sieves and stored under an inert atmosphere over molecular sieves. SciOPP ligand was prepared according to the literature method,[26] and dpbz, dppe, and Xantphos were purchased from Strem and used as received. $FeCl_2$(SciOPP), $FeCl(dpbz)_2$, and $FeCl(dppe)_2$ were prepared using literature procedures.[26,31] All iron(II) bisphosphine complexes in this study were moderately air sensitive, whereas all iron(I) bisphosphines were highly air sensitive.

5.2. Mössbauer Spectroscopy. Solid state samples were prepared in an inert atmosphere glovebox equipped with a liquid nitrogen fill port to allow sample freezing to 77 K within the glovebox. Each sample was loaded into a Delrin Mössbauer sample cup for measurements and loaded under liquid nitrogen. ^{57}Fe Mössbauer measurements were performed using a SeeCo MS4 Mössbauer spectrometer integrated with a Janis SVT-400T He/N_2 cryostat for measurements at 80 K with a 0.07 T applied magnetic field. Isomer shifts were determined relative to α-Fe at 298 K. All Mössbauer spectra were fit using the program WMoss (SeeCo).

5.3. Magnetic Circular Dichroism Spectroscopy. All samples for MCD spectroscopy were prepared in an inert atmosphere glovebox equipped with a liquid nitrogen fill port to allow sample freezing to 77 K within the glovebox. Frozen solution MCD samples were prepared in a 6:1 (v:v) toluene-d_8/benzene-d_6 mixture (mixtures used to afford low-temperature optical glasses) in copper cells fitted with quartz disks and a 3 mm gasket. For $FeCl_2$(Xantphos), solid state mulls were prepared using ground polycrystalline sample and paratone oil as a mulling agent. NIR MCD experiments were conducted using a Jasco J-730 spectropolarimeter and a liquid nitrogen-cooled InSb detector. The spectral range accessible with this NIR MCD setup is 2000−600 nm. UV−visible (UV−vis) MCD spectra were collected using a Jasco J-715 spectropolarimeter and a shielded S-20 photomultiplier tube. Both instruments utilize a modified sample compartment incorporating focusing optics and an Oxford Instruments SM4000-7T superconducting magnet/cryostat, permitting measurements from 1.6 to 290 K with magnetic fields of up to 7 T. A calibrated Cernox sensor directly inserted into the copper sample holder is used to measure the temperature at the sample to ±0.001 K. All MCD spectra were baseline-corrected against zero-field scans. VTVH-MCD spectra were analyzed using previously reported fitting procedures.[50,51] For VTVH-MCD fitting, both negative and positive zero-field splitting models were evaluated. The reported error bars were determined via evaluation of the effects of systematic variations of the fit parameters on the quality of the overall fit.

5.4. Electronic Structure Calculations. Spin-unrestricted density functional theory (DFT) calculations were performed with the Gaussian 09 package.[52] All geometry optimization calculations were performed with the PBEPBE[53] exchange-correlation functional with the TZVP[54] basis set on all atoms with the inclusion of solvation effects using the polarized continuum model (PCM) with toluene as the solvent[55] with the exception of $FeCl_2$(Xantphos) for which no solvent model was included (to correlate with the obtained solid state spectroscopy for this complex). The geometries of all complexes were fully optimized starting from X-ray crystal structures with initial optimization performed with cep-31g before optimizing at the TZVP level. All optimized geometries had frequencies found to be real. Energies given in the Supporting Information include zero-point and thermal corrections. Further calculations of MOs and TD-DFT analysis used the spin-unrestricted B3LYP functional with the TZVP basis set on all atoms. MO compositions, analyzed via Mulliken population analysis, and calculation of Mayer bond orders were performed using the AOMix program.[56,57] Calculated MOs were plotted with the ChemCraft program. TD-DFT was used to calculate electronic transition energies for the 80−100 lowest-energy states.

5.4.1. 1,2-Bis(3,5-di-tert-butylphenylphosphino)ethane (^{tBu}dppe). 3,5-Di-*tert*-butylphenylmagnesium bromide was prepared by stirring 4.34 g of 3,5-di-*tert*-butylbromobenzene (16.1 mmol) and 502 mg of Mg^0 (20.7 mmol, 1.3 equiv) in 50 mL of THF under gentle heat for 12 h. The mixture was filtered to remove excess Mg^0, and the filtrate was added dropwise to a stirring, prechilled (−65 °C) solution of 1,2-bis(dichlorophosphino)ethane (852 mg, 3.7 mmol) in 25 mL of THF. After completion of addition, the reaction mixture was stirred at −65 °C for 1 h and then allowed to warm to room temperature while being stirred for an additional 4 h. The solvent was then removed under reduced pressure and the off-white crude solid redissolved in dichloromethane (50 mL) and washed with saturated $(NH_4)_2SO_4$ (50 mL). The aqueous layer was then separated and extracted with dichloromethane (3 × 50 mL portions). The combined organic layers were then washed with brine (150 mL). The organic phase was separated, dried over $MgSO_4$, and filtered, and the solvent was removed under reduced pressure. The resulting solid was sonicated in 50 mL of MeOH and isolated by filtration as a colorless powder: yield 2.70 g (87%); ^{1}H NMR (400 MHz, THF-d_8, 298 K) δ 1.26 (s, 72H), 2.11 (s, 4H), 7.24 (s, 8H), 7.38 (s, 4H); ^{31}P{^{1}H} NMR (162 MHz, THF-d_8, 298 K) δ −8.84 (relative to external 85% H_3PO_4). Elemental Anal. Calcd: C, 82.22; H, 10.47. Found: C, 81.55; H, 10.55. Slow cooling of a hot 2-propanol solution of ^{tBu}dppe to room temperature afforded colorless crystals suitable for X-ray analysis.

5.4.2. $FeCl_2$(dpbz). A 100 mL round-bottom flask was charged with 80 mg of $FeCl_2{\cdot}THF_{1.5}$ (0.3 mmol) along with 25 mL of toluene. To a separate scintillation vial were added 152 mg of dpbz (0.3 mmol) and 10 mL of toluene. Both vessels were stirred while being heated to 85 °C, followed by the dropwise addition of the hot solution of ligand to the hot stirring iron suspension. The resulting mixture was allowed to stir for 4 h at 85 °C, by which time the reaction mixture had become a pale yellow solution. The hot solution was filtered through a pad of Celite, and the filtrate was allowed to cool to room temperature before being divided into two equal fractions and stored at −30 °C. After 3 days, colorless block-shaped X-ray quality crystals had precipitated from solution and were isolated by filtration from both fractions: yield 0.100 g (51%). Elemental Anal. Calcd for $FeCl_2$(dpbz) and 0.5 equiv of toluene: C, 64.97; H, 4.56. Found: C, 64.91; H, 4.48. The slightly higher analyzed C value coincides with observation of cocrystallized solvent during X-ray analysis. ^{57}Fe Mössbauer values (solid, 80 K): δ = 0.73 mm/s, and ΔE_Q = 2.49 mm/s.

5.4.3. $FeCl_2$(^{tBu}dppe). A 500 mL round-bottom flask was charged with 214 mg of $FeCl_2{\cdot}THF_{1.5}$ (0.9 mmol, 851 mg), ^{tBu}dppe (1.0 mmol, 1.1 equiv), and 200 mL of 2-propanol. The mixture was stirred at reflux for 6 h, after which the reaction mixture was allowed to cool to room temperature and the solvent removed under reduced pressure. The resulting solid was redissolved in 50 mL of dichloromethane and the solution filtered through a pad of Celite. Removal of the solvent under reduced pressure resulted in a white solid that was subsequently washed with cold hexane (10 mL, three times) and isolated by filtration: yield 670 mg (76%). Elemental Anal. Calcd: C, 71.52; H, 9.11. Found: C, 71.65; H, 9.09. ^{57}Fe Mössbauer values (solid, 80 K): δ = 0.73 mm/s, and ΔE_Q = 2.82 mm/s. X-ray quality crystals were grown from slow evaporation of a concentrated 1,4-dioxane solution of the complex.

5.4.4. $FeCl_2$(Xantphos). A 50 mL round-bottom flask was charged with 95 mg of $FeCl_2{\cdot}THF_{1.5}$ (0.40 mmol), 250 mg of Xantphos (1.1 equiv, 0.43 mmol), and 20 mL of toluene. The mixture was stirred for 4 h at 60 °C by which time a white precipitate was produced. The reaction mixture was cooled to room temperature and filtered, and the isolated white powder was washed with cold (−30 °C) THF (3 mL). Concentrating the complex in THF and allowing for slow evaporation at room temperature afford colorless block crystals suitable for X-ray analysis: yield 280 mg (100%). Elemental Anal. Calcd: C, 66.41; H, 4.57. Found: C, 66.30; H, 4.63. ^{57}Fe Mössbauer values (solid, 80 K): δ = 0.75 mm/s, and ΔE_Q = 2.67 mm/s.

5.4.5. [FeBr(SciOPP)]$_2$. To a stirring solution of $FeBr_2$(SciOPP) (60 mg, 0.054 mmol) dissolved in 4 mL of diethyl ether cooled to −80 °C

DOI: 10.1021/acs.inorgchem.5b02263
Inorg. Chem. XXXX, XXX, XXX−XXX

was added 8.7 mg of KC_8 (1.2 equiv, 0.064 mmol) in approximately 2 mg portions. The resulting dark green solution was allowed to stir for 10 min at −80 °C and then filtered through Celite to remove solid graphite and unreacted KC_8. The reaction vial was sealed with Apiezon N grease and transferred to a −80 °C freezer. After 2 weeks, a few crystals of red-orange crystalline solid precipitated and the highly temperature sensitive crystals were analyzed by X-ray crystallography. Insufficient material combined with the high temperature sensitivity of this species precluded additional characterization.

■ ASSOCIATED CONTENT

Supporting Information

The Supporting Information is available free of charge on the ACS Publications website at DOI: 10.1021/acs.inorgchem.5b02263.

Supplementary figures and data, including ^{57}Fe Mössbauer, UV−vis MCD, and ^{1}H and ^{31}P NMR spectra, MO diagrams, and TD-DFT analyses (PDF)

X-ray crystal structure details (CIF)

■ AUTHOR INFORMATION

Corresponding Author

*E-mail: neidig@chem.rochester.edu.

Notes

The authors declare no competing financial interest.

■ ACKNOWLEDGMENTS

This work was supported by a grant from the National Institutes of Health (R01GM111480 to M.L.N.). The authors thank Dr. William W. Brennessel for assistance in the collection and analysis of X-ray crystallographic data and Malik Al-Afyouni for assistance in preliminary studies. Further acknowledgement is extended to the Center for Integrated Research Computing at the University of Rochester for providing the resources necessary for performing the computational work presented in this study.

■ REFERENCES

(1) Bolm, C.; Legros, J.; Le Paih, J.; Zani, L. *Chem. Rev.* **2004**, *104*, 6217.

(2) Czaplik, W. M.; Mayer, M.; Cvengros, J.; von Wangelin, A. J. *ChemSusChem* **2009**, *2*, 396−417.

(3) Sherry, B. D.; Fürstner, A. *Acc. Chem. Res.* **2008**, *41*, 1500.

(4) Bedford, R. B. *Acc. Chem. Res.* **2015**, *48*, 1485−1493.

(5) Bauer, I.; Knolker, H.-J. *Chem. Rev.* **2015**, *115*, 3170−3387.

(6) Jana, R.; Pathak, T. P.; Sigman, M. S. *Chem. Rev.* **2011**, *111*, 1417−1492.

(7) Tamura, M.; Kochi, J. K. *J. Am. Chem. Soc.* **1971**, *93*, 1487−1489.

(8) Tamura, M.; Kochi, J. K. *J. Organomet. Chem.* **1971**, *31*, 289−309.

(9) Tamura, M.; Kochi, J. K. *Bull. Chem. Soc. Jpn.* **1971**, *44*, 3063−3073.

(10) Neumann, S. M.; Kochi, J. K. *J. Org. Chem.* **1975**, *40*, 599−606.

(11) Smith, R. S.; Kochi, J. K. *J. Org. Chem.* **1976**, *41*, 502−509.

(12) Nakamura, M.; Matsuo, K.; Ito, S.; Nakamura, E. *J. Am. Chem. Soc.* **2004**, *126*, 3686−3687.

(13) Guérinot, A.; Reymond, S.; Cossy, J. *Angew. Chem., Int. Ed.* **2007**, *46*, 6521−6524.

(14) Cahiez, G.; Duplais, C.; Moyeux, A. *Org. Lett.* **2007**, *9*, 3253−3254.

(15) Noda, D.; Sunada, Y.; Hatakeyama, T.; Nakamura, M.; Nagashima, H. *J. Am. Chem. Soc.* **2009**, *131*, 6078−6079.

(16) Bedford, R. B.; Betham, M.; Bruce, D. W.; Danopoulos, A. A.; Frost, R. M.; Hird, M. *J. Org. Chem.* **2006**, *71*, 1104−1110.

(17) Ghorai, S.; Jin, M.; Hatakeyama, T.; Nakamura, M. *Org. Lett.* **2012**, *14*, 1066−1069.

(18) Hatakeyama, T.; Nakamura, M. *J. Am. Chem. Soc.* **2007**, *129*, 9844−9845.

(19) Hatakeyama, T.; Hashimoto, S.; Ishizuka, K.; Nakamura, M. *J. Am. Chem. Soc.* **2009**, *131*, 11949−11963.

(20) Guisán-Ceinos, M.; Tato, F.; Bunuel, E.; Calle, P.; Cardenas, D. J. *Chem. Sci.* **2013**, *4*, 1098−1104.

(21) Przyojski, J. A.; Veggeberg, K. P.; Arman, H. S.; Tonzetich, Z. J. *ACS Catal.* **2015**, *5*, 5938−5946.

(22) Hatakeyama, T.; Kondo, Y.; Fujiwara, Y.; Takaya, H.; Ito, S.; Nakamura, E.; Nakamura, M. *Chem. Commun.* **2009**, 1216−1218.

(23) Bedford, R. B.; Brenner, P. B.; Carter, E.; Clifton, J.; Cogswell, P. M.; Gower, N. J.; Haddow, M. F.; Harvey, J. N.; Kehl, J. A.; Murphy, D. M.; Neeve, E. C.; Neidig, M. L.; Nunn, J.; Snyder, B. E. R.; Taylor, J. *Organometallics* **2014**, *33*, 5767−5780.

(24) Dongol, K. G.; Koh, H.; Sau, M.; Chai, C. L. L. *Adv. Synth. Catal.* **2007**, *349*, 1015−1018.

(25) Hatakeyama, T.; Hashimoto, T.; Kathriarachchi, K. K. A. D. S.; Zenmyo, T.; Seike, H.; Nakamura, M. *Angew. Chem., Int. Ed.* **2012**, *51*, 8834−8837.

(26) Hatakeyama, T.; Hashimoto, T.; Kondo, Y.; Fujiwara, Y.; Seike, H.; Takaya, H.; Tamada, Y.; Ono, T.; Nakamura, M. *J. Am. Chem. Soc.* **2010**, *132*, 10674−10676.

(27) Hatakeyama, T.; Fujiwara, Y.; Okada, Y.; Itoh, T.; Hashimoto, T.; Kawamura, S.; Ogata, K.; Takaya, H.; Nakamura, M. *Chem. Lett.* **2011**, *40*, 1030−1032.

(28) Hatakeyama, T.; Okada, Y.; Yoshimoto, Y.; Nakamura, M. *Angew. Chem., Int. Ed.* **2011**, *50*, 10973−10976.

(29) Sun, C.-L.; Krause, H.; Fürstner, A. *Adv. Synth. Catal.* **2014**, *356*, 1281−1291.

(30) Bedford, R. B.; Huwe, M.; Wilkinson, M. C. *Chem. Commun.* **2009**, 600−602.

(31) Adams, C. J.; Bedford, R. B.; Carter, E.; Gower, N. J.; Haddow, M. F.; Harvey, J. N.; Huwe, M.; Cartes, M. A.; Mansell, S. M.; Mendoza, C.; Murphy, D. M.; Neeve, E. C.; Nunn, J. *J. Am. Chem. Soc.* **2012**, *134*, 10333−10336.

(32) Bedford, R. B.; Carter, E.; Cogswell, P. M.; Gower, N. J.; Haddow, M. F.; Harvey, J. N.; Murphy, D. M.; Neeve, E. C.; Nunn, J. *Angew. Chem., Int. Ed.* **2013**, *52*, 1285−1288.

(33) Bedford, R. B.; Brenner, P. B.; Carter, E.; Carvell, T. W.; Cogswell, P. M.; Gallagher, T.; Harvey, J. N.; Murphy, D. M.; Neeve, E. C.; Nunn, J.; Pye, D. R. *Chem. - Eur. J.* **2014**, *20*, 7935−7938.

(34) Gartner, D.; Stein, A. L.; Grupe, S.; Arp, J.; Jacobi von Wangelin, A. *Angew. Chem., Int. Ed.* **2015**, *54*, 10545−10549.

(35) Mayer, M.; Czaplik, W. M.; Jacobi von Wangelin, A. *Adv. Synth. Catal.* **2010**, *352*, 2147−2152.

(36) Czaplik, W. M.; Mayer, M.; Jacobi von Wangelin, A. *ChemCatChem* **2011**, *3*, 135−138.

(37) Daifuku, S. L.; Al-Afyouni, M. H.; Snyder, B. E. R.; Kneebone, J. L.; Neidig, M. L. *J. Am. Chem. Soc.* **2014**, *136*, 9132−9143.

(38) Daifuku, S. L.; Kneebone, J. L.; Snyder, B. E. R.; Neidig, M. L. *J. Am. Chem. Soc.* **2015**, *137*, 11432−11444.

(39) Hermes, A. R.; Girolami, G. S. *Inorg. Chem.* **1988**, *27*, 1775−1781.

(40) Neumeyer, F.; Lipschutz, M. I.; Tilley, T. D. *Eur. J. Inorg. Chem.* **2013**, *2013*, 6075−6078.

(41) Higham, L. J.; Middleton, A. J.; Heslop, K.; Pringle, P. G.; Barber, A.; Guy Orpen, A. *J. Organomet. Chem.* **2004**, *689*, 2963−2968.

(42) Liu, T.; DuBois, D. L.; Bullock, R. M. *Nat. Chem.* **2013**, *5*, 228−233.

(43) Mankad, N. P.; Whited, M. T.; Peters, J. C. *Angew. Chem., Int. Ed.* **2007**, *46*, 5768−5771.

(44) O'Reilly, R. K.; Shaver, M. P.; Gibson, V. C.; White, A. J. P. *Macromolecules* **2007**, *40*, 7441−7452.

(45) Grutters, M. M. P.; van der Vlugt, J. I.; Pei, Y.; Mills, A. M.; Lutz, M.; Spek, A. L.; Muller, C.; Moberg, C.; Vogt, D. *Adv. Synth. Catal.* **2009**, *351*, 2199−2208.

(46) Schreiter, W. J.; Stanley, G. G.; Fronczek, F. R. CCDC 1014733. Private communication to the Cambridge Structural Database, 2014.

DOI: 10.1021/acs.inorgchem.5b02263
Inorg. Chem. XXXX, XXX, XXX−XXX

(47) Langer, R.; Bönisch, F.; Maser, L.; Pietzonka, C.; Vondung, L.; Zimmermann, T. P. *Eur. J. Inorg. Chem.* **2015**, *2015*, 141−148.
(48) $[(\mu\text{-dppe})FeCl_2]_n$ was found also to be accessible by stirring equimolar dppe and $FeCl_2(THF)_{1.5}$ in THF at room temperature. Concentration of the resulting solution and layering with pentane allowed the isolation of colorless crystals with a structure matching that of coordination polymer **1′** in ref 47.
(49) Fillman, K. L.; Przyojski, J. A.; Al-Afyouni, M. H.; Tonzetich, Z.; Neidig, M. L. *Chem. Sci.* **2015**, *6*, 1178−1188.
(50) Pavel, E. G.; Kitajima, N.; Solomon, E. I. *J. Am. Chem. Soc.* **1998**, *120*, 3949−3962.
(51) Neese, F.; Solomon, E. I. *Inorg. Chem.* **1999**, *38*, 1847−1865.
(52) Frisch, M. J.; Trucks, G. W.; Schlegel, H. B.; Scuseria, G. E.; Robb, M. A.; Cheeseman, J. R.; Scalmani, G.; Barone, V.; Mennucci, B.; Petersson, G. A.; Nakatsuji, H.; Caricato, M.; Li, X.; Hratchian, H. P.; Izmaylov, A. F.; Bloino, J.; Zheng, G.; Sonnenberg, J. L.; Hada, M.; Ehara, M.; Toyota, K.; Fukuda, R.; Hasegawa, J.; Ishida, M.; Nakajima, T.; Honda, Y.; Kitao, O.; Nakai, H.; Vreven, T.; Montgomery, J. A., Jr.; Peralta, J. E.; Ogliaro, F.; Bearpark, M.; Heyd, J. J.; Brothers, E.; Kudin, K. N.; Staroverov, V. N.; Kobayashi, R.; Normand, J.; Raghavachari, K.; Rendell, A.; Burant, J. C.; Iyengar, S. S.; Tomasi, J.; Cossi, M.; Rega, N.; Millam, M. J.; Klene, M.; Knox, J. E.; Cross, J. B.; Bakken, V.; Adamo, C.; Jaramillo, J.; Gomperts, R.; Stratmann, R. E.; Yazyev, O.; Austin, A. J.; Cammi, R.; Pomelli, C.; Ochterski, J. W.; Martin, R. L.; Morokuma, K.; Zakrzewski, V. G.; Voth, G. A.; Salvador, P.; Dannenberg, J. J.; Dapprich, S.; Daniels, A. D.; Farkas, Ö.; Foresman, J. B.; Ortiz, J. V.; Cioslowski, J.; Fox, D. J. *Gaussian 09*, revision D.01; Gaussian, Inc.: Wallingford, CT, 2013.
(53) Perdew, J. P.; Burke, K.; Ernzerhof, M. *Phys. Rev. Lett.* **1996**, *77*, 3865−3868.
(54) Schäfer, A.; Huber, C.; Ahlrichs, R. *J. Chem. Phys.* **1994**, *100*, 5829−5835.
(55) Tomasi, J.; Mennucci, B.; Cammi, R. *Chem. Rev.* **2005**, *105*, 2999−3094.
(56) Gorelsky, S. I. *AO Mix: Program for Molecular Orbital Analysis*, version 6.8.5, 2014 (http://www.sg-chem.net/).
(57) Gorelsky, S. I.; Lever, A. B. P. *J. Organomet. Chem.* **2001**, *635*, 187−196.

DOI: 10.1021/acs.inorgchem.5b02263
Inorg. Chem. XXXX, XXX, XXX−XXX